

Robust Physical Hard-Label Attacks on Deep Learning Visual Classification

Ryan Feng¹, Jiefeng Chen², Earleence Fernandes², Somesh Jha², Atul Prakash¹

¹University of Michigan, Ann Arbor, ²University of Wisconsin, Madison

¹{rtfeng, aprakash}@umich.edu, ²{jiefeng, earleence, jha}@cs.wisc.edu

Abstract

The physical, black-box hard-label setting is arguably the most realistic threat model for cyber-physical vision systems. In this setting, the attacker only has query access to the model and only receives the top-1 class label without confidence information. Creating small physical stickers that are robust to environmental variation is difficult in the discrete and discontinuous hard-label space because the attack must both design a small shape to perturb within and find robust noise to fill it with. Unfortunately, we find that existing ℓ_2 or ℓ_∞ minimizing hard-label attacks do not easily extend to finding such robust physical perturbation attacks. Thus, we propose GRAPHITE, the first algorithm for hard-label physical attacks on computer vision models. We show that “survivability”, an estimate of physical variation robustness, can be used in new ways to generate small masks and is a sufficiently smooth function to optimize with gradient-free optimization. We use GRAPHITE to attack a traffic sign classifier and a publicly-available Automatic License Plate Recognition (ALPR) tool using only query access. We evaluate both tools in real-world field tests to measure its physical-world robustness. We successfully cause a Stop sign to be misclassified as a Speed Limit 30 km/hr sign in 95.7% of physical images and cause errors in 75% of physical images for the ALPR tool.

1 Introduction

Machine learning (ML) models, such as deep-neural networks (DNNs), have had resounding success in several scenarios such as face and object recognition [15, 17, 34, 36, 38]. Based on this success, they are now a part of perception pipelines in cyber-physical systems (CPSs) like cars [12, 20, 28], UAVs [2, 25] and robots [41]. However, recent work has found that these models are vulnerable to attacks such as test-time adversarial examples [5, 14, 30, 39], where an adversary subtly perturbs a benign input to cause a misclassification by the ML model.

Recent work in the computer vision community has made progress in understanding the space of adversarial



(a) Targeted GTSRB attack to convert a Stop sign into a Speed Limit 30 km/hr sign.



(b) Physical license plate holder sticker attack to make ALPR fail to correctly read the plate. Plate was purchased online.

Figure 1: Example GRAPHITE attacks.

examples, beginning in the digital domain and more recently, in the physical domain where attackers can perturb physical objects by printing stickers or colorful patterns [1, 4, 10, 35]. Existing physical approaches currently rely on white-box access. Independently, researchers have begun exploring black-box hard-label attacks that operate in the digital domain [3, 6, 8, 9, 16], where attackers only have query access to the model to obtain the top-1 class label without any confidence information. For the first time, we tackle both challenges in the much more difficult but more realistic *physical hard-label case*, where attackers must generate physical stickers with only query access.

We observe that this threat model more closely mirrors real-world ML deployments — many commercial or proprietary systems are closed source and only provide class labels as output. For example, the PlateRecognizer [31] Automatic License Plate Recognition (ALPR) system offers a paid service that includes a closed source vision ML model, with only a label predictive API exposed. Similarly, Keen Lab’s recent security analysis of auto-wipers on a Tesla shows that even with significant reverse engineering effort, it is difficult to completely reconstruct a deployed model due to proprietary formats, implementations, and stripped binaries [19], whereas obtaining query access is much easier. Imposing hard-label access represents perhaps the weakest but most realistic threat model, as it is the minimum amount of information an ML model, including a

proprietary one, has to make available for it to be useful. An automatic physical perturbation generation pipeline could then be useful for testing closed-source supplier-provided models against realistic attacks.

An ideal attack would, with only hard-label access, efficiently generate adversarial perturbations in small, automatically determined areas with high survivability and minimal target artifacts (where “survivability” refers to the expected attack success rate under physical-world transforms). One key challenge is achieving high survivability — traditionally obtained with Expectation over Transformation (EoT) [1] — without gradients. As we show in Table 1, including an EoT-based loss function in OPT-attack [8], a distance-reformulated digital hard-label attack, is inefficient and leaves *undesirable artifacts* that reveal the intended target label to a human observer.

A second challenge is “*mask generation*”, where we must design small masks to restrict the area where the perturbation can be added to the underlying object, to emulate sticker or graffiti-style attacks. Even existing white-box work (RP₂ [10]) does not have a fully automatic process and requires significant manual experimentation to find good masks. In hard-label settings, the problem is even harder. Adapting ℓ_2 or ℓ_∞ -minimizing digital hard-label attacks to reduce mask size (an ℓ_0 type of problem) is difficult because ℓ_0 is non-differentiable. We further note that the attack starting point is important because no further information is gained while optimizing unless the decision boundary is identifiable. Digital ℓ_2 or ℓ_∞ hard-label attacks solve this by interpolating along the vector from the victim image to the target image [8], which ensures the boundary is always reached along this direction. Moving along that vector does not change the mask size and thus is not helpful in finding a good decision boundary for reducing mask size. Furthermore, for a given mask, interpolation may never find a decision boundary unless one can find at least one content to fill the the mask with that causes a misclassification. Thus, the current hard-label attack methods do not directly apply to physical perturbation attacks.

To address these challenges, we propose a new *survivability-based* approach named GRAPHITE (Generating Robust Adversarial Physical Hard-label Image Test Examples), the first (to our knowledge) algorithm that generates physically robust adversarial examples for computer vision systems in the hard-label setting. We design a joint optimization problem that encompasses mask and perturbation generation and propose algorithms to solve it in two stages. In particular, we show that our proposed survivability-based reformulation creates a *sufficiently smooth* objective for GFO to optimize. GRAPHITE also *automatically* generates masks (i.e., perturbation position, shape and size) with a survivability-based heatmap and mask reduction algorithm.

We generate GRAPHITE attacks on a traffic sign clas-

sifier and a real-world commercial automated license plate recognition (ALPR) system for which we only have hard-label query access. To evaluate our attacks, we perform domain-appropriate *field tests* to measure physical-world robustness. While digital survivability is a useful proxy, it is important to evaluate in the real-world to get a truer measure of physical robustness. Specifically, we print stickers on real, true-to-scale traffic signs and cars and measure under a variety of viewpoints and lighting conditions. We make this distinction between our realistic *field tests* with actual objects at realistic physical imaging conditions and generic *physical tests*, which include printed posters or objects not necessarily even to scale.

We evaluate 710 field test images and show that we can attack a Stop sign to be misclassified as a variety of other traffic signs (including a Speed Limit 30 km/hr sign in 95.7% of images). To show generalizability, we generate digital results for all 1806 GTSRB victim target pairs and get an average survivability of 77.8%. We also successfully induce errors in up to 82.5% of cases for ALPR. We note that ALPR systems can be misused for mass surveillance purposes [11], and that our hard-label attacks could be used to evade such surveillance and maintain privacy. Example physical attacks are shown in Fig. 1.

Our Contributions:

- We introduce GRAPHITE, the first physical adversarial attack in the black-box hard-label setting. We propose a novel optimization objective and provide algorithms to find robust attacks *even in the discrete and discontinuous hard-label setting*. We show that survivability is a sufficiently smooth function to optimize with gradient-free optimization.
- We present a novel mask generation process to *automatically* generate candidate masks that spatially constrain perturbations in the black-box hard-label setting.
- We evaluate effectiveness of GRAPHITE on multiple scenarios including attacks on models for classifying traffic signs as well as recognizing license plates (in the latter, just by perturbing the small area normally occupied by a license plate holder). We perform both digital and real-world field tests.

2 Related Work

Physical attacks on computer vision. Existing work for robust physical perturbation attacks on computer vision is in the *white-box* setting. Examples include printing images of perturbed objects [18], modifying objects with stickers [10, 35], and 3D printing perturbed objects [1]. Such

attacks typically optimize the expectation over a distribution of transformations, known as *Expectation over Transformation (EoT)* [1]. Such transformations model changes in viewing angle, distance, lighting, etc. In this work, we describe the expectation of attack success over such transformations as the *survivability* of an attack. Some attacks also introduce the notion of a mask that constrains the perturbation to small regions of the object [10]. However, existing work does not fully automatically generate suitable masks, and the mask is not jointly optimized with the noise.

In contrast, we construct robust, physical attacks with only top-1 hard-label information, enabling us to attack real-world systems. We additionally generate our masks automatically in a joint optimization problem.

Digital black-box attacks.

- **Transfer Attack:** These techniques train a surrogate model, generate white-box examples on the surrogate, and hope they transfer to the target [29]. Unfortunately, targeted examples often fail to transfer [22]. Many techniques also require access to similar training sets that may not be available, whereas our work only requires query access to the target model.
- **Soft-label Attack:** These *score-based* techniques require access to the softmax layer output in addition to class labels [7, 26]. Using this information, they can apply zeroth-order optimization or local search strategies to compute the adversarial example. In contrast, our threat model only allows the attacker top-1 predicted class label access.
- **Hard-label Attack:** Recent work has explored *digital* hard-label attacks [3, 6, 8, 9, 16], where only the top-1 label prediction is available. Such attacks are difficult because the hard-label optimization space is discontinuous and discrete. One approach is to reformulate the objective into a continuous optimization problem that finds the perturbation direction at which the decision boundary is closest. This approach is taken by OPT-attack [8], which uses the Randomized Gradient Free (RGF) method [13, 27] to optimize this distance-based objective. The boundary distance is calculated through a binary search process. The perturbation is initialized by interpolating with a target class image.

In our work, we generate physically robust examples within small masked areas with only hard-label access. As we show in Section 5.2, directly adding EoT to this distance-based reformulation is both inefficient and ineffective, leaving visible artifacts of the intended target. Unlike OPT-attack, we also generate masks.

3 Optimizing Hard-Label Physical Attacks

In this section, we will describe optimization problems for our approach, GRAPHITE. We want GRAPHITE to, without gradients, find a small candidate mask and perturbation within that masked area so that the resulting image is likely to be robust when physically realized. We also want GRAPHITE to be efficient and not have obvious target image artifacts. We will first describe a joint optimization problem for finding an optimal perturbation and mask, and then discuss a two-stage process that is more practical for the hard-label setting. The first stage finds an appropriate mask, and then the second stage optimizes the perturbation with RGF [27] in a survivability-based reformulation.

As in Athalye *et al.* [1], we also rely on estimating *survivability* of an image under transforms, i.e., the expectation of an image being predicted with a given label under physical transformations (this was termed EoT in Athalye *et al.* [1]). Details on the specific transformations used are included in the supplementary material (Section B).

3.1 Problem Setup

In our approach, our goal is to find some perturbation δ and a small mask M such that when δ is applied to a victim image x our model F predicts the target label y_{tar} with high survivability. The area that δ may occupy is constrained by the mask M . The perturbations must have high expected survivability under transformations t sampled from a distribution T . For initialization, we utilize an example target image x_{tar} . We constrain the perturbation by limiting its size, rather than minimizing a norm. Note that the output of F is the hard-label prediction. We describe a targeted attack formulation, but can easily adapt to untargeted.

3.2 Joint Optimization of Mask and Perturbation

We will first describe our new joint optimization problem for finding a robust perturbation δ to pixels within a masked area M that results in the target label y_{tar} . The optimal noise must maximize survivability (i.e., EoT) and, ideally, take up as little of the sign as possible. M_{ij} is 1 if pixel at position (i, j) is perturbed and 0 otherwise. These goals are in opposition and must be solved jointly to achieve the best solution ($\lambda > 0$ is the relative weight given to size of the mask M in the joint objective).

$$\operatorname{argmin}_{\delta, M} \lambda \cdot \|M\|_0 - \mathbb{E}_{t \sim T} \left[F \left(t(x + M \cdot \delta) \right) = y_{tar} \right] \quad (1)$$

We observe that solving this objective is challenging, especially in the hard-label setting — finding an optimally-sized mask within a graph is itself an NP-complete problem

(proof in Section C of supplementary material). One approach to constructing such masks is to adopt an ℓ_0 “heuristic” (the ℓ_0 norm itself is fundamentally non-differentiable, so straightforward adaptations of OPT-attack cannot be used). As an example, JSMA [30] builds a mask by considering the pixels most “relevant” towards causing a misclassification. However, this relevancy is traditionally determined by observing the gradient of the model output (logits) for the target class with respect to each pixel. Such a process cannot be directly applied to the hard-label setting because small changes in pixels are unlikely to change the top-1 hard label. To confirm this, we find that a patch version of this fails to generate survivable masks as described in supplementary Section A.3. In light of these observations, we instead solve a *decoupled optimization problem*.

3.3 Two-Step Optimization

Step #1: Mask Generation: We first find an optimized mask that, when filled in with the target image x_{tar} , results in at least a specified level of survivability, s_{lo} , a hyperparameter. We constrain the unmasked perturbation to be fixed at $\delta_{tar} = x_{tar} - x$ and solve the optimization objective from (1) under that constraint:

$$\begin{aligned} \operatorname{argmin}_M \lambda \cdot \|M\|_0 - \mathbb{E}_{t \sim T} \left[F \left(t(x + M \cdot \delta_{tar}) \right) = y_{tar} \right] \\ \text{s.t. } \mathbb{E}_{t \sim T} \left[F \left(t(x + M \cdot \delta_{tar}) \right) = y_{tar} \right] \geq s_{lo} \end{aligned} \quad (2)$$

We show how to solve this formulation heuristically using an algorithm described in Section 4.1. Note that δ_{tar} is only applicable within the resulting mask M . (See intermediate output after Mask Generation in Figure 2).

Step #2: Boosting via Perturbation Generation: Equipped with the mask M found by the Mask Generation Optimization Problem in Step #1, we then aim to maximize survivability for the given mask by changing the perturbation δ within the masked region (see final output in Figure 2 for an example result):

$$\operatorname{argmax}_{\delta} \mathbb{E}_{t \sim T} \left[F \left(t(x + M \cdot \delta) \right) = y_{tar} \right] \quad (3)$$

By using survivability as a measure of physical robustness (which we estimate with Equation 4), we can leverage this function as an optimization goal we can pursue even in the hard-label case (described in Section 4.2). In Section 4.3, we provide empirical evidence that this survivability-based reformulation is approximately continuous. We do this by showing that the objective has relatively low Lipschitz constants even when approximating the expectation in (3) by averaging over n transformations. We additionally refer to

this process as *boosting* the survivability, as we attempt to boost the survivability as high as we can.

4 Generating Hard-Label Physical Attacks with GRAPHITE

We now describe how to solve the mask and perturbation generation problems presented in Section 3 in the hard-label setting. For ease of algorithmic notation, given a mask M and perturbation δ the survivability in (3) can be estimated by computing n randomly sampled transformations $t_i \sim T$:

$$S_{x,y_{tar}}(M, \delta) = \frac{\sum_{i=1}^n \mathbb{1} \left[F \left(t_i(x + M \cdot \delta) \right) = y_{tar} \right]}{n} \quad (4)$$

Fig. 2 shows the algorithm flow along with intermediate and final results. The figure covers the mask generation and boosting phases we will discuss next.

4.1 Mask Generation

We need to find a candidate mask that has good initial survivability and small size. Boosting can take care of further improving the survivability as long as it samples enough variance at nearby points to make useful gradient estimates with RGF. In this phase, we set the perturbation to the target image’s pixels within the mask. In other words, the resulting image at this stage is $x + M \cdot (x_{tar} - x)$.

We generate masks using a three stage process:

1. Heatmap Estimation
2. Coarse-grained Mask Reduction
3. Fine-grained Mask Reduction

We first initialize the mask to the entire victim object, which overlays the target object over the victim. We then choose a group of pixels called a *patch* as a configurable input into the algorithm. We then collect all patches of a given shape (e.g. 4×4 squares) that overlap with the victim object. These patches serve two purposes: (1) it helps us estimate a “heatmap” (i.e., which regions of pixels contribute more to survivability) and (2) it is used to remove groups of pixels from the mask to reduce its size as the algorithm optimizes the mask objective function (2).

This process can be visualized by imagining a thin overlay of the target being placed on top of the victim, and then slowly cutting regions out of the overlay, exposing the victim object underneath.

Heatmap Estimation. We first generate a “heatmap” (similar to a saliency map) over the victim image. For each patch p that overlaps with the victim object, we measure the

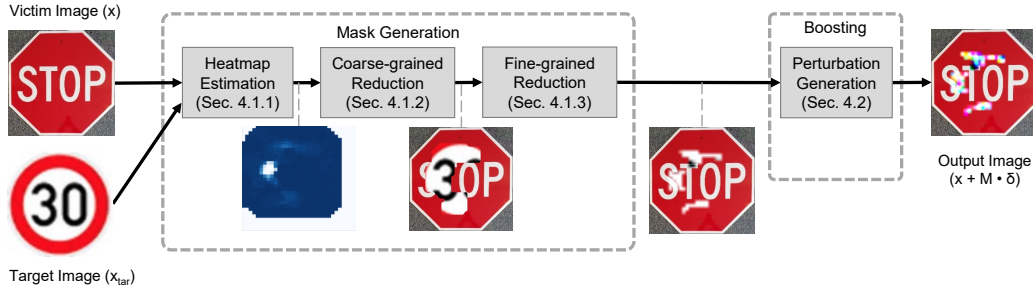


Figure 2: Figure showing the algorithm flow for a targeted attack on a Stop sign to Speed Limit 30 km / hr sign. Multiple transformations are sampled and used at each stage.

survivability of the mask M and perturbation δ_{tar} , where M includes every pixel of the victim object except for p . In other words, we take the original target image overlay, cut out p , and measure the resulting survivability. If the survivability drops a lot after removing p , those target pixels are important to causing a target prediction. This enables us to identify candidate regions to remove from the mask. We refer to this drop in survivability as the *impact* of that patch and output the sorted list of patches in increasing impact.

The size of the patches matters in the hard-label setting. If we pick just a single pixel as our patch, the survivability will likely be the same with or without it, making the heatmap useless. If we make the patch too large, we lose the ability to make more general mask shapes. For 32×32 noise, we empirically found that a 4×4 square patch worked well. Example heatmaps and discussion points are in the supplementary material (Section A.3).

Coarse-grained Mask Reduction. Using the sorted list of patches from heatmap estimation, we begin reducing the size of the mask. As an optimization to save queries, we first do a coarse-grained reduction that binary searches for a pivot in the patch list. Specifically, we find the point *pivot* in the ordered list of patches \mathcal{P} such that the bitwise unions of patches from that point ($\bigcup_{i=pivot}^{|\mathcal{P}|} \mathcal{P}_i$) yields a mask of survivability $\geq s_{hi}$, where s_{hi} is a hyper-parameter specifying a high survivability threshold that must be reached. If s_{hi} cannot be reached, we simply include all patches. Coarse-grained reduction outputs L_c , the list of patches from *pivot* to the end.

Fine-grained Mask Reduction. We then execute a fine-grained reduction that uses a greedy algorithm to improve the objective function of (2). Fine-grained reduction takes L_c and evaluates each patch in sorted order. It removes the patch if its removal improves the objective function and keeps it otherwise. Empirically, we found that it was important to add the restriction that survivability does not cross below some minimum threshold, s_{lo} to ensure success in boosting. The end result is the final mask defined by the

union of the retained elements of L_c . Because the objective function rewards small masks and high survivability, the final mask balances both well.

Let n be the number of transforms used for estimating survivability (per (4)). Heatmap estimation uses $n \cdot |\mathcal{P}|$ queries, coarse-grained reduction uses $n \cdot \log |\mathcal{P}|$ queries, and fine-grained reduction uses $n \cdot |L_c|$ queries.

4.2 Perturbation Generation (Boosting)

Given a resulting image x and a mask M from the previous stage, survivability boosting, or simply *boosting*, aims to find the perturbation δ that survives, in expectation, the most physical-world transformations. We propose a *survivability-based* reformulation to use with RGF [13, 27] to find the perturbation within the mask M with maximum survivability, which works as follows.

The perturbation δ is first initialized to $M \cdot (x_{tar} - x)$ and then we proceed to maximize the probability that a perturbation will remain robust to physical-world transforms with the RGF [13, 27] method for gradient estimation using q random samples for each gradient estimation. Explicitly, let u be random Gaussian unit vectors within the allowable range of the mask and let β be a nonzero smoothing parameter. Then, we set δ to $\delta - \eta \cdot \hat{g}$ where η is the step size and \hat{g} is the gradient, calculated as follows:

$$\hat{g} = \frac{S(M, \delta + \beta u) - S(M, \delta)}{\beta} \cdot u \quad (5)$$

Our survivability-based reformulation has two key benefits. First, we find experimentally that it leaves fewer obvious artifacts of the target image (see Table 1). Secondly, it is also more query-efficient than OPT-attack as it can measure survivability directly. RGF requires frequent computations of the objective, which is survivability in our case and boundary distance in OPT-attack. Calculating the boundary distance in OPT-attack requires performing query-intensive binary search operations while we do not.

Finally, we introduce the notion of a query budget which limits the amount of queries used in a particular stage of

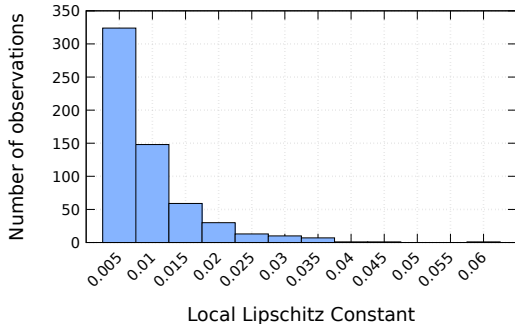


Figure 3: A histogram of our approximate local Lipschitz constant observations on survivability. This graph shows that survivability does not vary too much per amount of change with a sufficient number of transformations.

the algorithm. These parameters can be tuned to emphasize better mask generation or better boosting without a budget of queries if we want to limit the number of attack queries.

4.3 Suitability of Survivability Reformulation

To demonstrate that our survivability-based reformulation is approximately continuous for successful RGF optimization, we show empirically that our objective has a low local Lipschitz constant. We execute boosting on attack examples from `Stop` sign to `Speed Limit 30 km/hr`, `Stop` sign to `Pedestrians`, and `Stop` sign to `Turn Left Ahead` with $n = 1000$ transformations and approximate the local Lipschitz constant every time we compute $S(M, \delta + \beta \cdot u)$. The approximate local Lipschitz constant is given by $\frac{|S(M, \delta + \beta \cdot u) - S(\delta)|}{|\beta \cdot u|}$. We found that the maximum observed local Lipschitz constant was 0.056. We include a histogram of observed local Lipschitz constants in Fig. 3.

5 Experiments

We demonstrate the viability of GRAPHITE by attacking a traffic sign classifier trained on German Traffic Sign Recognition Benchmark (GTSRB) [37] data and by attacking a real-world ALPR system. We first report digital survivability results on all 1806 possible victim target pairs in GTSRB. Then, we print stickers on a smaller subset of attacks conduct real-world field tests to show that our results carry over to robustness in real-world field tests. We analyze over 700 field test images over three signs and two ALPR attacks under a variety of viewpoint and lighting conditions. We also compare against digital OPT-attack and a simple OPT+EoT extension attack as baselines.

Table 1: Baseline comparisons. GRAPHITE query counts include mask generation + boosting, baselines only boost. GRAPHITE results only use 20k queries in boosting. Baselines generated in 32×32 , GRAPHITE in 244×244 . ℓ_2 distances all calculated on 32×32 versions of the image.

OPT Attack Baseline	OPT + EoT Baseline	GRAPHITE
		
29.4k queries 3.78 ℓ_2 dist. 1% surv.	42.2k queries 7.83 ℓ_2 dist. 84% surv.	126.8k queries 10.2 ℓ_2 dist. 86% surv.
		
103.1k queries 1.08 ℓ_2 dist. 1% surv.	74.4k queries 8.23 ℓ_2 dist. 18% surv.	142.8k queries 10.7 ℓ_2 dist. 79% surv.
		
142.0k queries 1.29 ℓ_2 dist. 1% surv.	87.2k queries 9.77 ℓ_2 dist. 73% surv.	123.5k queries 7.85 ℓ_2 dist. 80% surv.

5.1 Experimental Setup

Datasets and Classifiers. We use the classifier from RP_2 [10, 40] trained on an augmented GTSRB dataset [37]. As with RP_2 [10], we replace the German `Stop` signs with U.S. `Stop` signs from the LISA dataset [24]. As a validation set, we take out the last 10% from each class in the training set. We augment the dataset with random rotation, translation, and shear, following Eykholt *et al.* [10]. Our network, GTSRB-Net, has a 97.656% test set accuracy.

In both attacks, we use our own victim image of the source object and use an Internet image outside of the dataset for initialization to demonstrate that GRAPHITE does not rely on having training set images to initialize from. In our experiments we assume that object boundaries are available, but note they could be obtained automatically through an object segmentation network [33].

For ALPR, we use OpenALPR version 2.3.0, the latest freely available version. We treat this command line tool as a complete black-box. While this particular tool provides confidence info, others may not so we discard that info during our attack. We initialize with the same image but with a gray rectangle filled in with (127, 127, 127) over the plate.

Table 2: Quantitative results of digital GTSRB attacks. Average and standard deviation of survivability, # of pixels out of $32 \times 32 = 1024$ in the mask (i.e., ℓ_0 distance), number of queries reported for the given victim to all other targets.

Victim	Stop	SL 30 km/hr	Avg. of all 43 victims
Surv. (%)	80.8±7.02	84.5±10.6	77.8±17.5
Mask Size	116±38.0	139±71.7	170.3±122
# Queries	133k±8.92k	134k±15.2k	126k±18.9k

More details about hyper-parameters are included in the supplementary material (Section A.1).

GTSRB Attack Details. We set the size of our input images to be 244×244 and used 100 randomly chosen transformations in the attack. During the attack, we generate 32×32 perturbations and then upsample to the resolution of the input image whenever they have to be added together.

For field testing, we print stickers and place them on a $30'' \times 30''$ Stop sign and it at stationary positions to test how robust our attacks are to different viewing conditions. We take five pictures of the perturbed Stop sign at 14 different locations for a total of 70 pictures. To test lighting conditions, we take one set of images in outdoor light and two sets indoors, one with indoor lights on and one without. To compare against baseline Stop sign accuracy, we also take five pictures of a clean Stop sign at each of the same 14 locations. The 14 locations were chosen based on RP_2 evaluation [10].

To gather crops we use the original author’s YOLOv3 [32] object detector network trained on MS COCO [21] to predict bounding boxes for the Stop sign. We take the output bounding boxes, crop the sign, resize to 32×32 , and send to our network for classification.

ALPR Attack Details. To attack ALPR systems, we imagine printing a license plate holder sticker to cause the ALPR system to fail to detect your license plate number correctly (in an untargeted fashion). In this case, we could attack with just the boosting stage from the (known) border mask consisting of the license plate holder, but this may lead to poor initial survivability. So, we alternate between mask generation and boosting in multiple rounds. More details are included in the supplementary material in Section A.

To test our ALPR attack, we print out the license plate holder stickers and place it on expired license plates we acquired for purposes of field testing. We ran ALPR on stationary pictures of the car taken in a driveway and took five pictures of the car at 5’, 10’, 15’, and 20’ away at both 0 and 15 degree angles. We generate our attack on images of height 500. The perturbation was generated at a height of

250 and enlarged to fit over the whole image.

As with GTSRB, we use the original author’s YOLOv3 [32] object detector network trained on MS COCO [21] to predict bounding boxes for the car. We take the output bounding boxes, crop the sign accordingly, and send the crops to the black-box ALPR pipeline.

5.2 Experimental Results

Baseline Comparisons. We compare our results to digital OPT-attack and OPT+EoT baselines. For the OPT+EoT baseline, we take digital OPT-attack and average the gradient direction over 100 transformations and otherwise leave the attack the same. The results for 3 attacks, Stop sign to Speed Limit 30 km/hr, Stop sign to Pedestrians, and Stop sign to Turn Left Ahead, are shown in Table 1.

GRAPHITE generally uses a comparable amount of queries compared to either baseline, despite using most of its queries on its extra mask generation step. The GRAPHITE results in Table 1 only used 20k queries in boosting. Compared to the digital OPT-attack baseline, GRAPHITE also solves a much harder problem in yielding physically survivable results. We also point out that the OPT+EoT baseline yields much worse artifacts across the entire image of the target image compared to GRAPHITE without using significantly fewer queries in most cases. Thus, GRAPHITE is much more suited to this problem than the naive OPT + EoT baseline.

Digital Survivability Results. We report digital results for all 1806 possible GTSRB victim target pairs in Table 2. We used a high threshold $s_{hi} = 85\%$ for coarse-grained mask reduction and a low threshold $s_{lo} = 65\%$ for fine-grained mask reduction. We find that on average we get masks with an ℓ_0 distance of 170.3 (w.r.t. 32×32) and 77.8% survivability. Images of additional attacks are included in the supplementary material (Section A.3).

Physical Survivability Field Tests. We also conducted physical object perturbation experiments in the field to confirm that our results carry over to physical survivability. We evaluate GRAPHITE on a targeted Stop sign attacks to targets of Speed Limit 30 km/hr, Pedestrians, and Turn Left Ahead at different viewing angles and lighting conditions. We also evaluate ALPR license plate holder attacks on two plates and cars. In total, we evaluated over 700 physical images.

- **GTSRB Results:** Table 3 shows the results of the field tests for GTSRB. On average, they took 131k queries. The Speed Limit 30 km/hr attack was successful over all three lighting conditions with at

Table 3: GTSRB field test results. Physical survivability results are calculated over 5 pictures each at the following spots: 5 ft \times {0°, 15°, 30°, 45°}, 10 ft \times {0°, 15°, 30°}, 15 ft \times {0°, 15°}, 20 ft \times {0°, 15°}, 25 ft, 30 ft, 40 ft. Each example was tested 3 times: outdoors, indoors with indoor lights turned off, and indoors with indoor lights turned on.

Victim	Target	Digital GRAPHITE attack	Physical GRAPHITE attack (outdoors)	Dig. Surv. (100 xforms)	Phys. Surv. (Indoors, lights off)	Phys. Surv. (Indoors, lights on)	Phys. Surv. (Outdoors)
				86%	92.9%	94.3%	100%
				79%	97.1%	85.7%	100%
				80%	55.7%	55.7%	0%

least 92.9% survivability. The Pedestrians attack also did well, with at least 85.7% success rate over each lighting condition. The Turn Left Ahead attack did less well, getting 55.7% indoors and 0% outdoors. As we discuss in Section 6, this is likely due to an inability to print dark blues and sun glare. Digitally darkening the outdoor images raises the success rate to 52.9%. Overall, these results suggest that digital survivability translates reasonably well into the physical world and improvements in transformations could further increase this. Baseline Stop sign tests were at least 95.7% in each lighting condition. We include extended field test results that characterize attack success under additional imaging conditions in Section A.2 of the supplementary material.

- **ALPR Results:** Table 4 shows ALPR field test results. These attacks took an average of 12950 queries. We found these attacks to have physical success as well. The Washington plate attack success rate was 82.5%. The digital attack success rate (survivability) for this attack was 80%. 100% of unperturbed, baseline images correctly predicted the license plate. For the Michigan plate attack, the attack succeeded in 67.5% of images while the digital survivability for this attack was 86%. 82.5% of unperturbed, baseline images correctly predicted the license plate. The average Levenshtein distance, which calculates the number of additions, subtractions, and substitutions required to change one string to another, was 2.175 (including correct predictions). These results also suggest that digital survivability translates to physical-world robustness.

6 Discussion

One limitation is printing error. We found that printing blue was more difficult than other colors. This is particularly clear in the perturbation over the “P” for the Turn Left Ahead attack, and likely explains the lesser performance. We found it difficult to improve the printing quality by adding the NPS term as in RP₂ [10].

A second key limitation is modeling sun glare. This can be seen in comparing the physical survivability rates of the Turn Left Ahead attack indoors vs. outdoors. While modeling gamma correction helps some with brightness changes, a better way to model sun glare specifically in EoT could help improve survivability.

We also developed a white-box version of GRAPHITE (with automatic mask generation) inspired by the C&W ℓ_0 attack [5]. This could represent a step towards physical adversarial training as a physical attack defense. More details are included in Section D of the supplementary material.

7 Conclusion

We developed GRAPHITE, the first algorithm for hard-label physical attacks on computer vision networks. With our survivability-based approach, we automatically generate small masks and then boost the perturbation with a smooth, survivability-based optimization. Through real-world field testing, we demonstrate feasible perturbations for attacking a traffic sign classifier and an automated license plate recognition (ALPR) system, bridging the gap to being able to attack real-world models in the more realistic hard-label physical setting.

Table 4: ALPR field test results. Survivability results calculated over 5 pictures each at: $\{5 \text{ ft}, 10 \text{ ft}, 15 \text{ ft}, 20 \text{ ft}\} \times \{0^\circ, 15^\circ\}$. License plates are expired plates we acquired for the purpose of testing these attacks. All images cropped to show the plate area in larger detail.

Digital GRAPHITE attack	Physical GRAPHITE attack	Phys. Surv.	Avg. Lev. Dist.
		82.5%	3.175
		67.5%	1.175

Acknowledgement

This material is based on work supported by DARPA under agreement number 885000, Air Force Grant FA9550-18-1-0166, the National Science Foundation (NSF) Grants 1646392, CCF-FMitF-1836978, SaTC-Frontiers-1804648 and CCF-1652140, and ARO grant number W911NF-17-1-0405. Earlence Fernandes is supported by the University of Wisconsin-Madison Office of the Vice Chancellor for Research and Graduate Education with funding from the Wisconsin Alumni Research Foundation. The U.S. Government is authorized to reproduce and distribute reprints for Governmental purposes notwithstanding any copyright notation thereon. Any opinions, findings, and conclusions or recommendations expressed in this material are those of the author(s) and do not necessarily reflect the views of our research sponsors.

References

- [1] Anish Athalye, Logan Engstrom, Andrew Ilyas, and Kevin Kwok. Synthesizing robust adversarial examples. *arXiv preprint arXiv:1707.07397*, 2017. **1, 2, 3, 14, 16**
- [2] Haitham Bou-Amr, Holger Voos, and Wolfgang Ertel. Controller design for quadrotor uavs using reinforcement learning. In *Control Applications (CCA), 2010 IEEE International Conference on*, pages 2130–2135. IEEE, 2010. **1**
- [3] Wieland Brendel, Jonas Rauber, and Matthias Bethge. Decision-based adversarial attacks: Reliable attacks against black-box machine learning models. *arXiv preprint arXiv:1712.04248*, 2017. **1, 3**
- [4] Tom B. Brown, Dandelion Mané, Aurko Roy, Martín Abadi, and Justin Gilmer. Adversarial patch. *arXiv preprint arXiv:1712.09665*, 2017. **1**
- [5] Nicholas Carlini and David Wagner. Towards evaluating the robustness of neural networks. In *2017 IEEE Symposium on Security and Privacy (SP)*, pages 39–57. IEEE, 2017. **1, 8, 12, 16**
- [6] Jianbo Chen, Michael I Jordan, and Martin J Wainwright. Hopskipjumpattack: A query-efficient decision-based attack. *arXiv preprint arXiv:1904.02144*, 2019. **1, 3**
- [7] Pin-Yu Chen, Huan Zhang, Yash Sharma, Jinfeng Yi, and Cho-Jui Hsieh. Zoo: Zeroth order optimization based black-box attacks to deep neural networks without training substitute models. In *Proceedings of the 10th ACM Workshop on Artificial Intelligence and Security*, pages 15–26. ACM, 2017. **3**
- [8] Minhao Cheng, Thong Le, Pin-Yu Chen, Jinfeng Yi, Huan Zhang, and Cho-Jui Hsieh. Query-efficient hard-label black-box attack: An optimization-based approach. In *International Conference on Learning Representations*, 2019. **1, 2, 3, 11, 14**
- [9] Minhao Cheng, Simranjit Singh, Pin-Yu Chen, Sijia Liu, and Cho-Jui Hsieh. Sign-opt: A query-efficient hard-label adversarial attack. *arXiv preprint arXiv:1909.10773*, 2019. **1, 3, 14**
- [10] Kevin Eykholt, Ivan Evtimov, Earlence Fernandes, Bo Li, Amir Rahmati, Chaowei Xiao, Atul Prakash, Tadayoshi Kohno, and Dawn Song. Robust Physical-World Attacks on Deep Learning Visual Classification. In *Computer Vision and Pattern Recognition (CVPR)*, June 2018. **1, 2, 3, 6, 7, 8, 10, 11, 14**
- [11] Electronic Frontier Foundation. Street-Level Surveillance: Automated License Plate Readers (ALPRs). <https://www.eff.org/pages/automated-license-plate-readers-alpr>. **2**
- [12] Andreas Geiger, Philip Lenz, and Raquel Urtasun. Are we ready for autonomous driving? the kitti vision benchmark suite. In *Computer Vision and Pattern Recognition (CVPR), 2012 IEEE Conference on*, pages 3354–3361. IEEE, 2012. **1**
- [13] Saeed Ghadimi and Guanghui Lan. Stochastic first-and zeroth-order methods for nonconvex stochastic programming. *SIAM Journal on Optimization*, 23(4):2341–2368, 2013. **3, 5, 11**
- [14] Ian J Goodfellow, Jonathon Shlens, and Christian Szegedy. Explaining and harnessing adversarial examples. *arXiv preprint arXiv:1412.6572*, 2014. **1**
- [15] Kaiming He, Xiangyu Zhang, Shaoqing Ren, and Jian Sun. Deep residual learning for image recognition. In *Proceedings of the IEEE conference on computer vision and pattern recognition*, pages 770–778, 2016. **1**
- [16] Andrew Ilyas, Logan Engstrom, Anish Athalye, and Jessy Lin. Black-box adversarial attacks with limited queries and information. In *Proceedings of the 35th International Conference on Machine Learning*, pages 2137–2146, 2018. **1, 3**
- [17] Alex Krizhevsky, Ilya Sutskever, and Geoffrey E Hinton. Imagenet classification with deep convolutional neural networks. In *Advances in neural information processing systems*, pages 1097–1105, 2012. **1**

- [18] Alexey Kurakin, Ian Goodfellow, and Samy Bengio. Adversarial examples in the physical world. *arXiv preprint arXiv:1607.02533*, 2016. **2**
- [19] Tencent Keen Security Lab. Experimental Security Analysis of Tesla AutoPilot. https://keenlab.tencent.com/en/whitepapers/Experimental_Security_Research_of_Tesla_Autopilot.pdf. **1**
- [20] Timothy P Lillicrap, Jonathan J Hunt, Alexander Pritzel, Nicolas Heess, Tom Erez, Yuval Tassa, David Silver, and Daan Wierstra. Continuous control with deep reinforcement learning. *arXiv preprint arXiv:1509.02971*, 2015. **1**
- [21] Tsung-Yi Lin, Michael Maire, Serge Belongie, James Hays, Pietro Perona, Deva Ramanan, Piotr Dollár, and C Lawrence Zitnick. Microsoft coco: Common objects in context. In *European conference on computer vision*, pages 740–755. Springer, 2014. **7**
- [22] Yanpei Liu, Xinyun Chen, Chang Liu, and Dawn Song. Delving into transferable adversarial examples and black-box attacks. *CoRR*, abs/1611.02770, 2016. **3**
- [23] Aleksander Madry, Aleksandar Makelov, Ludwig Schmidt, Dimitris Tsipras, and Adrian Vladu. Towards deep learning models resistant to adversarial attacks. *arXiv preprint arXiv:1706.06083*, 2017. **16**
- [24] Andreas Mogelmoose, Mohan Manubhai Trivedi, and Thomas B Moeslund. Vision-based traffic sign detection and analysis for intelligent driver assistance systems: Perspectives and survey. *IEEE Transactions on Intelligent Transportation Systems*, 13(4):1484–1497, 2012. **6**
- [25] Christian Mostegel, Markus Rumlper, Friedrich Fraundorfer, and Horst Bischof. Uav-based autonomous image acquisition with multi-view stereo quality assurance by confidence prediction. In *Proceedings of the IEEE Conference on Computer Vision and Pattern Recognition Workshops*, pages 1–10, 2016. **1**
- [26] Nina Narodytska and Shiva Kasiviswanathan. Simple black-box adversarial attacks on deep neural networks. In *2017 IEEE Conference on Computer Vision and Pattern Recognition Workshops (CVPRW)*, pages 1310–1318, July 2017. **3**
- [27] Yurii Nesterov and Vladimir Spokoiny. Random gradient-free minimization of convex functions. *Foundations of Computational Mathematics*, 17(2):527–566, 2017. **3, 5**
- [28] OpenPilot. OpenPilot on the Comma Two. <https://github.com/commaai/openpilot>, 2020. **1**
- [29] Nicolas Papernot, Patrick McDaniel, and Ian Goodfellow. Transferability in machine learning: from phenomena to black-box attacks using adversarial samples. *arXiv preprint arXiv:1605.07277*, 2016. **3**
- [30] Nicolas Papernot, Patrick McDaniel, Somesh Jha, Matt Fredrikson, Z Berkay Celik, and Ananthram Swami. The limitations of deep learning in adversarial settings. In *2016 IEEE European symposium on security and privacy (EuroS&P)*, pages 372–387. IEEE, 2016. **1, 4, 12**
- [31] Plate Recognizer. Plate Recognizer Automatic License Plate Recognition Software. <https://platerrecognizer.com/>. **1**
- [32] Joseph Redmon and Ali Farhadi. Yolov3: An incremental improvement. *arXiv preprint arXiv:1804.02767*, 2018. **7, 11**
- [33] Olaf Ronneberger, Philipp Fischer, and Thomas Brox. U-net: Convolutional networks for biomedical image segmentation. In *International Conference on Medical image computing and computer-assisted intervention*, pages 234–241. Springer, 2015. **6**
- [34] Florian Schroff, Dmitry Kalenichenko, and James Philbin. Facenet: A unified embedding for face recognition and clustering. In *Proceedings of the IEEE conference on computer vision and pattern recognition*, pages 815–823, 2015. **1**
- [35] Mahmood Sharif, Sruti Bhagavatula, Lujo Bauer, and Michael K. Reiter. Accessorize to a crime: Real and stealthy attacks on state-of-the-art face recognition. In *Proceedings of the 2016 ACM SIGSAC Conference on Computer and Communications Security, CCS '16*, page 1528–1540, 2016. **1, 2**
- [36] Karen Simonyan and Andrew Zisserman. Very deep convolutional networks for large-scale image recognition. *arXiv preprint arXiv:1409.1556*, 2014. **1**
- [37] Johannes Stalkamp, Marc Schlipfing, Jan Salmen, and Christian Igel. Man vs. computer: Benchmarking machine learning algorithms for traffic sign recognition. *Neural networks*, 32:323–332, 2012. **6, 11**
- [38] Christian Szegedy, Vincent Vanhoucke, Sergey Ioffe, Jon Shlens, and Zbigniew Wojna. Rethinking the inception architecture for computer vision. In *Proceedings of the IEEE conference on computer vision and pattern recognition*, pages 2818–2826, 2016. **1**
- [39] Christian Szegedy, Wojciech Zaremba, Ilya Sutskever, Joan Bruna, Dumitru Erhan, Ian Goodfellow, and Rob Fergus. Intriguing properties of neural networks. *arXiv preprint arXiv:1312.6199*, 2013. **1**
- [40] Vivek Yadav. p2-traffic signs. <https://github.com/vxy10/p2-TrafficSigns>, 2016. **6**
- [41] Fangyi Zhang, Jürgen Leitner, Michael Milford, Ben Uppcroft, and Peter Corke. Towards vision-based deep reinforcement learning for robotic motion control. *arXiv preprint arXiv:1511.03791*, 2015. **1**

Appendices

We include additional experimental and theoretical material in this supplementary document. In Section **A** we include additional field tests, experiments, and experimental details. In Section **B** we provide details on our physical world transforms. Section **C** includes a proof on mask generation NP-completeness. Finally, Section **D** provides details on a white-box version of GRAPHITE that we recently developed, which unlike RP_2 [10], also automatically generates small masks but like RP_2 , aims to get robust perturbations, which have high survivability. We include initial comparisons of results from black-box (hard-label) and white-box adversarial attack generation.

A Experimental Details

A.1 Hyper-parameters.

We set the smoothing parameter $\beta = 1$, step size $\eta = 500$, and the boosting query budget b to 20k. For both GTSRB and ALPR, we test over $n = 100$ transformations to compute survivability and take $q = 10$ gradient samples for RGF sampling [13]. For transformations, we model rotations about the y axis with homography matrices, lighting changes with gamma correction, and focus changes with Gaussian blurring.

For our GTSRB [37] attack we set rotation about the y axis to be between -50° and 50° and fix the base focal length $f = 3$ ft. The projected image plane distance is allowed to vary between f and 15 ft. Crop sizes and offsets can vary between 0% and 3.125%. The max γ effect can be 3.5 for darkening (or $\frac{1}{3.5}$ for lightening), and use Gaussian kernels of size 1, 5, and 9. All parameters are sampled uniformly. We set λ in Equation 2 to 5.

For our ALPR attack, we set rotation to be between -15° and 15° and fix the base focal length $f = 10$ ft. We set the Gaussian kernels to sizes 1, 3, and 5, and let the remaining parameters match the GTSRB attack. We used 3 iterations of mask generation and boosting. The patch size for mask generation was 8×8 , then 4×4 , and then in the last iteration the mask was fixed to just the border. The stride for the patches was the width divided by 2. We additionally added in the backtracking line search to adaptively select the step size as in OPT-attack [8]. We set $s_{lo} = 20\%$ and $s_{hi} = 60\%$. We use $n = 10$ transforms in mask generation and $n = 50$ transforms in boosting. We set λ in Equation 2 to 25.

A.2 Extended Field Test Experimentation

In this section, we provide extended field test results for GTSRB under additional imaging conditions. In particular, we record videos while driving towards the sign in a private lot, simulating a realistic driving environment in an allowable fashion¹. We test each of the three attacks from Table 3. As in prior work by Eykholt et al. [10], we analyze every 10th frame from the video. We use the same YOLOv3 [32] detector as the other GTSRB results to crop our frames. Some frames, particularly ones at the beginning of the video when we were farthest away could not be cropped with YOLOv3 and were thus cropped manually in a similar fashion.

We include results for these three stop sign attacks in Table 6. The Speed Limit 30 km/hr attack was the most successful, with 97.5% survivability, which is inline

¹We follow local laws and regulations for safety in this test.

Table 5: Sample of extended GTSRB field test pictures. TOP: Speed Limit 30 km/hr attack. MIDDLE: Pedestrians attack. BOTTOM: Turn Left Ahead attack.



Table 6: Extended GTSRB field test results, including the measured physical survivability of the video frames. Every 10th frame of the videos were analyzed.

Target	# Frames Analyzed	Attack Success Rate (Survivability)
Speed Limit 30 km/hr	40	97.5%
Pedestrians	39	82.1%
Turn Left Ahead	42	19.0%

with the field test results in Table 3 and above the digital survivability. The Pedestrians attack was also successful with an 82.1% survivability rate, which is right around the its digital survivability of 79%. The Turn Left Ahead attack was also fairly successful at 19.0% given its 0% rate in the outdoor field test results in Table 3. Overall, these results confirm the field test results reported in Table 3 in an even more realistic driving setting.

With regards to the Turn Left Ahead sign, the indoor and outdoor field-test results in Table 3 and Table 6 suggest a higher sensitivity to lighting conditions (e.g., higher attack success in indoor lighting vs. outdoors in sunlight). Our conjecture is that, as noted in the discussion in the Experiments and Discussion section in the main paper, this particular attack relies more heavily on presence of deep blues in the perturbation area. Our data suggests that, because of both color printer’s limitations and sun glare issues, deep blue color is particularly difficult for a camera to reproduce in different lighting conditions. To add on to that point here, the color in the blue spot over the “P” includes the tuple (0, 0, 255) frequently but our camera sensed it as around (96, 157, 211) in the drive-by tests. Our transforms do attempt to adjust for lighting changes using random transforms from a well-known technique called gamma correction (for more details, see Section B). Gamma correction adjusts a color value as follows, given a value γ , either darkening it or making it lighter:

$$x_{out} = \left(\frac{x_{in}}{255}\right)^\gamma \cdot 255 \quad (6)$$

But it turns out that gamma correction will always fail to darken or brighten a (0, 0, 255) and leave it as (0, 0, 255). This suggests a limitation of using gamma correction as a method for modeling lighting changes (especially impact of sunlight) for colors at the extreme ends of the RGB spectrum; a better model to address lighting changes at extreme ends of the spectrum in EoT transforms may increase robustness. Note that when we did a test increase of contrast and decrease of brightness over the blue region by the “P”, in order to make the region a deeper blue, the attack success rate went up to 47.6%, with all of the last 11 analyzed frames plus 9 others being classified as Turn Left Ahead. This seems to back the hypothesis that the low fidelity in reproducing blues is causing issues. We also found that this attack was more successful in indoor lighting as shown in Table 3 than in outdoor tests, including drive-by experiments; blues were indeed reproduced better by our camera in indoor lighting.

A.3 Additional Results

This section includes additional analysis on heatmap estimation, digital survivability results, and an ablation study of mask reduction techniques.

Digital Survivability Results In Table 7 we provide results from attacks between all victim target pairs of a subset of 10 varied GTSRB signs. We include the final output image, the survivability, and the mask size. GRAPHITE generally finds small, highly survivable perturbations on a variety of attacks. The examples that tend to not perform as well are attacks on a triangle sign victim, as overcoming the difference in shape is difficult. Furthermore, it is not a large enough space to fit the entire target object on the victim, meaning that in reduction the starting survivability may be low to begin with, making it hard to prune patches from the mask. Resizing the target image to fit within the victim image may alleviate this concern. In general, we find the attack quality will vary depending on the victim target pair, which is consistent with prior work that finds that the distortion can drastically vary depending on the attack pair [30].

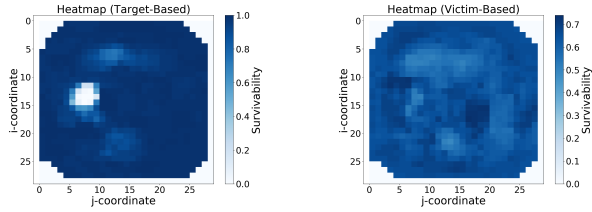
Heatmap Estimation In general, the heatmap is a function of the point at which it is estimated. The heatmap can also be computed relative to the target (as is done in our algorithm as described in Section 4.1) or relative to the victim. For a Stop sign to Speed Limit 30 km / hr attack, a relative to target heatmap overlaps a Speed Limit 30 km / hr over the Stop sign and sees the survivability drop by removing one patch of the 30 at a time. A relative to victim heatmap would take the Stop sign and try adding one patch of the Speed Limit 30 km / hr at a time. Fig. 4a shows the heatmap with respect to the target and Fig. 4b shows the heatmap relative to the victim. We found the victim heatmap to be ineffective because the survivability (with respect to the target label) tended to remain 0.

In principle, the heatmap could be measured at multiple points during the algorithm, but the measurement is expensive in terms of number of queries and computation time. Specifically, for example, we experimented with alternating between mask generation and boosting but found this to be extremely query expensive (e.g., 142.7k additional queries for only 4 pixels of reduction for three iterations on a Stop sign to Speed Limit 30 km/hr sign). Empirically, we found that just using one heatmap (in our case, the target one) worked well in practice. The white area in Fig. 4a is interesting – it suggests that area is likely to be crucial for applying a patch in order to convert the Stop sign to the Speed Limit 30 km/hr sign. Conversely, darker areas in Fig. 4a are good candidates for elimination from the mask.

Digital L_0 Experiments To demonstrate the difficulty of L_0 optimization in the hard-label setting (even with approaches such as JSMA [30] or C&W L_0 attack [5]), we run a simple experiment that runs our GRAPHITE pipeline with no transforms. In the hard-label setting, there is no

Table 7: Sample of digital targeted attacks on GTSRB-Net. Ran with $s_{lo} = 65\%$, $s_{hi} = 85\%$, $n = 100$ transforms. For cells with same victim and target, we report the % of transforms the original label is predicted. Masks size is reported in terms of # of pixels in 32×32 (i.e., L_0 in 32×32 space).

Victim	Target									
Survivability	92%	86%	85%	79%	80%	82%	80%	90%	77%	71%
Mask Size	0	88	123	105	51	96	131	92	138	97
Survivability	77%	100%	88%	94%	94%	89%	88%	99%	61%	93%
Mask Size	161	0	18	140	74	152	175	45	210	156
Survivability	79%	97%	88%	87%	88%	91%	95%	97%	62%	65%
Mask Size	171	13	0	228	132	173	162	41	213	122
Survivability	50%	73%	52%	95%	86%	79%	100%	0%	79%	88%
Mask Size	398	398	398	0	198	254	28	398	205	190
Survivability	73%	85%	71%	85%	100%	81%	71%	80%	71%	71%
Mask Size	111	72	120	92	0	122	93	74	263	148
Survivability	0%	58%	7%	4%	92%	100%	46%	87%	83%	57%
Mask Size	436	436	436	436	81	0	436	157	198	436
Survivability	56%	84%	70%	90%	80%	69%	100%	0%	78%	77%
Mask Size	398	398	398	23	133	225	0	398	133	161
Survivability	74%	91%	73%	86%	77%	78%	76%	99%	72%	69%
Mask Size	172	43	75	92	62	106	133	0	218	114
Survivability	72%	83%	82%	74%	91%	92%	78%	90%	73%	79%
Mask Size	142	123	141	159	137	137	175	90	0	182
Survivability	79%	89%	89%	81%	82%	67%	82%	91%	73%	99%
Mask Size	42	85	79	106	106	153	117	62	242	0



(a) Heatmap with respect to the target (Speed Limit 30 km / hr sign) (b) Heatmap with respect the victim (Stop sign)

Figure 4: Example heatmaps.

confidence or direct gradient information so for any sort of heatmap signal we rely on patch-based removal to see if the decision changes without that patch.

We run this pipeline for all victim target pairs from Table 7 in the supplementary material. We find that the average starting survivability of the output mask from mask generation with this setting is 4.18% and that 87.8% of the 90 cases (10 victims \times 10 targets minus the 10 cells that are the identity attacks) had less than 10% survivability. After boosting from this mask, we get an average of 12.3% and find that 78.9% of the cases had less than 20% final survivability. Thus, these types of L_0 approaches by themselves are not as good as our survivability based approach at solving mask generation.

We note that, state-of-the-art hard-label attack algorithms that rely on finding attacks, such as OPT-attack [8] and SIGN-OPT [9], aim to minimize ℓ_2 or ℓ_∞ -based measures for the size the perturbation with respect the original label. They thus can find a solution by first finding the optimal solution (based on binary search) in the vector direction $(x - x_0)$ from the victim image x_0 to an image x from another class – a point closer to x_0 along this vector will also tend to have a smaller perturbation with respect to ℓ_2 and ℓ_∞ norms. Binary search along that direction makes the interpolation algorithm query-efficient as well. Unfortunately, with an ℓ_0 -based distance measure, the points other than x_0 along the vector $x - x_0$ will all have the same norm. For example, if x is (2, 3, 4) and x_0 is (1, 2, 1), all points along the vector $x - x_0$, i.e., $(1, 2, 1) + \delta * (2, 1, 3)$ where $\delta \in (0, 1]$ will have an identical ℓ_0 norm of 3 with respect to x_0 . Thus, finding a decision-boundary along such a vector will not result in a small mask size and another approach is required.

We also note that OPT-attack [8] requires that a boundary be found. In the regular digital case, this is taken care of by the above interpolation of victim and target images; in the worst case, the algorithm can just take the entire target image to flip the decision (assuming the model predicts this natural target image correctly). However, with small masks, we cannot rely on such a guarantee. As an example, we try experimenting with the Speed Limit 80 km/hr mask

from RP_2^2 , setting the initial perturbation inside the mask to correspond to the target image. We conduct this experiment completely in 32×32 like a regular digital OPT-attack would be done for our GTSRBNet. We tried this strategy for every target and find that the resulting image is predicted as a Stop sign for every target, including Speed Limit 80 km/hr. In other words, OPT fails to properly initialize with that mask. We also try seeing if masks can transfer by taking the mask from GRAPHITE’s Stop sign Speed Limit 30 km/hr attack (which we note includes more pixels than the RP_2 test mask) and find that only 4 of the other 40 targets can be initialized this way. Thus, masks must be designed with good initial survivability in mind.

B Modeling Physical Transforms using Classical Computer Vision

Prior work by Eykholt et al. [10] and Athalye et al. [1] model environmental effects to create physical-world attacks in the white-box setting. These transformations account for varying conditions such as the distance and angle of the camera, lighting conditions, etc. Based on this work, we build a more principled set of transformations using classical computer vision techniques. To this end, we group these effects into 3 main classes of transformations:

1. **Geometric transformations:** These transformations refer to shape-based changes including rotation, translation and zoom. For planar objects, all three effects can be captured in a single perspective transformation through a homography matrix. Homography matrices relate two planar views under different perspectives.

Geometrically, to convert points from one image plane to another, one can break down the operation into a rotation and translation matrix R , perspective projection onto a plane (P), and an affine transformation from plane to pixels (A). In the planar case, this boils down to a 3×3 homography matrix H :

$$x_{out} = APRx_{in} = Hx_{in} \quad (7)$$

We use these homographies to simulate rotation around the y axis and different viewing distances for given ranges of values. Once we pick values for each of the parameters uniformly, we construct the homography matrix to compute the transformation.

After performing the perspective transform, we random crop to the tightest square crop that includes the whole object $\pm c\%$ of the resultant image size to adjust

²https://github.com/evtimovi/robust_physical_perturbations/blob/master/gtsrb-cnn-attack/masks/mask_llrectangles-less_256.png

for cropping errors. We also add random offsets for the crop, given as two more parameters. Then, we resize the square to the original resolution.

2. **Radiometric transformations:** These are appearance-based transformations with effects such as lighting-based changes. One technique to perform brightness adjustments is gamma correction, which applies a nonlinear function. Separately, printers apply nonlinear functions to their colorspace as well. Gamma correction is reflective of nonlinear human sight perception. To model these radiometric-based changes, we model gamma correction under gamma values between $\frac{1}{\gamma}$ and γ , with half coming from $[\frac{1}{\gamma}, 1]$ and half coming from $[1, \gamma]$ in expectation where γ is the maximum gamma value allowed. Assuming the image ranges from $[0, 1]$, this is defined as the following:

$$x_{out} = x_{in}^{\gamma} \quad (8)$$

Note that one limitation with gamma correction is that if the color consists of RGB values of 0 or 255, the color will not change regardless of the value of gamma.

3. **Filtering transformations:** These transformations model changes related to the camera focus. We model Gaussian blurring of different kernel sizes to measure the effects of the target object being out-of-focus. We note that as a side benefit, this may help deal with printer error as some precision in color values is lost in printing. To maximize this printer side benefit, we blur just the perturbation, and let the perspective transform take care of minor out of focus variation in the rest of the image.

We define a single transformation to be a composite function that includes one of each type of modeled transformation. In our case with those listed above, we would have a perspective transform followed by a cropping operation, gamma correction, and a Gaussian blur convolution. Examples of transformed images are shown in Figure 5.

C NP-Completeness of Mask Generation

A $n \times n$ square grid is represented as G_n , which is a graph (V_n, E_n) (V_n has vertices (i, j) , where $0 \leq i \leq n$ and $0 \leq j \leq n$ and for each (i, j) , $\{(i, j + 1), (i, j - 1), (i + 1, j), (i - 1, j)\} \cap V_n$ is in the set of edges E_n). A *mask* M is a sub-graph of the grid G_n that corresponds to a contiguous region of squares. Let $C(G_n)$ be the set of masks corresponding to the grid G_n . Let $\mu : C(G_n) \rightarrow \mathbb{R}^+$ be a *monotonic scoring function* ($M \subseteq M'$ implies that $\mu(M) \leq$



Figure 5: Examples of different transformed images. The upper-left image is the original, and the rest are three examples of transformed versions with perspective, lighting, and blurring transforms.

$\mu(M')$). The mask generation problem can be stated as follows: Given r and threshold t , find a mask M of size $\leq r$ (the size of the mask is number of squares in it) such that $\mu(M) \geq t$. We call this problem $\text{MASK}_P(n, \mu, r, t)$.

Simply enumerating masks is not feasible because the number of masks could be exponential. We provide a simple argument. Consider a $k \times k$ sub-grid of G_n . Consider columns that are odd numbered (i.e. of the form (i, \star) , where i is odd). Now any choice of one square for the even columns gives us a contiguous mask, so there are $\geq 2^{\frac{k(k+1)}{2}}$ masks. There are $(n - k)^2$ $k \times k$ sub-grids in G_n . So a lower bound on masks of size k is at least $(n - k)^2 2^{\frac{k(k+1)}{2}}$. Next we prove that our problem is actually NP-complete.

The Set Cover. Given a universe \mathcal{U} and a family \mathcal{S} of subsets of \mathcal{U} , a cover is a subfamily $\mathcal{C} \subseteq \mathcal{P}(\mathcal{U})$ of sets whose union is \mathcal{U} . In the set-covering decision problem, the input is a triple $(\mathcal{U}, \mathcal{S}, k)$ (k is an integer), and the question is *whether there is a set covering of size k or less*. In the set covering optimization problem, the input is a pair $(\mathcal{U}, \mathcal{S})$ and the task is to find a set covering that uses the fewest sets. The set-covering decision problem is known to be NP-complete.

Theorem 1 *Problem MASK_P is NP-complete.*

Proof. Our reduction will be from the decision set-cover problem. Assume we are given an instance of the set-cover problem $(\mathcal{U}, \mathcal{S}, k)$. Let $n = \max(|\mathcal{U}|, |\mathcal{S}|)$. We create a $n \times n$ grid G_n . Let $C(G_n)$ be the set of masks of G_n . We construct a scoring function μ as follows: Let M be a mask. Let $I = \{i | (i, 0) \in M\}$, and $\mathcal{S}_I = \{S_j | j \in I \wedge S_j \in \mathcal{S}_I\}$. $\mu(M) = 1$ if and only if the following condition holds (otherwise $\mu(M) = 0$): $|I| \leq k$ and $\cup_{j \in I} S_j = \mathcal{U}$. It is easy to see that $\text{MASK}_P(n, \mu, n^2, 1)$ has a satisfying solu-



Figure 6: Stop sign attacked using the white-box version of GRAPHITE, with target label as Speed Limit 30 km/hr.

tion iff the instance of the set cover problem has a solution. This proves that the problem is NP-hard. Given a solution to the problem $\text{MASK}_P(n, \mu, r, t)$, it is easy to check that it is a valid solution in polynomial time, so the problem is NP. Therefore, $\text{MASK}_P(n, \mu, r, t)$ is NP-complete. \square

D White-box Version and Adversarial Training

GRAPHITE is not only the first physical black-box hard-label attack, but also the first attempt at automating the mask-generation pipeline for physical adversarial examples. As such, we expand upon this contribution and offer an additional, preliminary automated mask-generation algorithm for the white-box setting. It is our expectation that defenses against physical adversarial examples might employ some form of adversarial training (as in the digital domain), and thus might benefit from such an algorithm.

Our white-box version is inspired by the Carlini-Wagner (C&W) L_0 attack [5]. The original algorithm greedily reduces the cardinality of the mask (allowed set of pixels that can be perturbed), alternating between pixel removal and running the C&W L_2 attack until the attack can no longer find an adversarial example. The attack determines impact with a heuristic: supposing that x is the input image and δ is the perturbation, it removes the pixel $i = \text{argmin}_i g_i \cdot \delta_i$, where g_i is the gradient of the loss with respect to the i^{th} pixel of the attacked image (i.e., $x + \delta$) and δ_i is the perturbation for that pixel from the attacked image. We modify this philosophy to reduce the cardinality of the mask until a white-box version of boosting can no longer achieve a minimum acceptable survivability of S_t . To adapt to the physical domain, we also remove patches of pixels rather than a single pixel at a time to encourage printable masks and for efficiency.

More specifically, we begin by initializing the mask (allowed set) of pixels to be all the pixels in the victim image. Then, we perform a round of *mask reduction*, which comprises 2 steps: (1) Constructing an adversarial example with EoT [1] and Projected Gradient Descent (PGD) [23],

and (2) removing the pixels from the mask that are least relevant in causing a misclassification. We compute the average impact of the patches (in just the areas that overlap with the current mask) and remove the z least impactful patches (a hyperparameter). For efficiency, each round begins with the previous round’s perturbation and then applies a random start of size. This process iteratively repeats until the final round, in which step (1) can no longer find an adversarial example with survivability greater than S_t within a reasonable number of PGD iterations.

We run a preliminary test of our algorithm on a Stop sign to Speed Limit 30 km/hr attack. We set $z = 4$ and $S_t = 85\%$, with both attack and evaluation survivability computed using 100 transforms. PGD is performed with a step-size of $2/255$, and a maximum of 50 iterations per round. We do not bound the norm of the perturbation and instead let the size of the mask minimize the perturbation. The input image is in 244×244 . To mimic GRAPHITE’s process of generating 32×32 perturbation, when taking a step in the direction of the sign of the gradient, we make the following modifications: the gradient is resized to 32×32 , we take the sign of the gradient, and then we resize it back to 244×244 to get the new gradient direction. We use a patch size of 30×30 with a stride of 10, which is approximately the size of the black-box patching conducted in 32×32 . Finally, our random start applies noise between $[-8/255, 8/255]$.

Figure 6 shows the final Stop sign to Speed Limit 30 km/hr white-box attack. The attack concluded in 43 rounds (approximately 2.5 minutes, compared to about 9.5 minutes for GRAPHITE) with a final survivability of 85%. The size of the mask, which was generated in 244×244 for the white-box version, is 2620 pixels (4.4% of the total image area). The black-box version computed the mask directly in 32×32 to model 32×32 perturbations, and GRAPHITE generated an attack with 88 pixels (which is 8.59% of the total image area).